A Chlorophyte Alga Utilizes Alternative Electron Transport for Primary Photoprotection[1][OPEN]

Maxwell A. Ware, Darcy Hunstiger, Michael Cantrell, and Graham Peers[2,3]

Department of Biology, Colorado State University, Fort Collins, Colorado 80523

ORCID IDs: 0000-0001-6551-8538 (M.A.W.); 0000-0003-3829-6233 (M.C.); 0000-0002-3590-7820 (G.P.).

The green alga *Desmodesmus armatus* is an emerging biofuel platform that produces high amounts of lipids and biomass in mass culture. We observed *D. armatus* in light-limiting, excess-light, and sinusoidal-light environments to investigate its photoacclimation behaviors and the mechanisms by which it dissipates excess energy. Chlorophyll *a*/*b* ratios and the functional absorption cross section of PSII suggested a constitutively small light-harvesting antenna size relative to other green algae. In situ and ex situ measurements of photo-physiology revealed that nonphotochemical quenching is not a significant contributor to photoprotection; however, cells do not suffer substantial photoinhibition despite its near absence. We performed membrane inlet mass spectrometry analysis to show that *D. armatus* has a very high capacity for alternative electron transport (AET) measured as light-dependent oxygen consumption. Up to 90% of electrons generated at PSII can be dissipated by AET in a water–water cycle during growth in rapidly fluctuating light environments, like those found in industrial-scale photobioreactors. This work highlights the diversity of photoprotective mechanisms present in algal systems, indicating that nonphotochemical quenching is not necessarily required for effective photoprotection in some algae, and suggests that engineering AET may be an attractive target for increasing the biomass productivity of some strains.

Photoprotective processes allow the reaction oxygenic photosynthesis to maintain relatively high efficiencies in fluctuating light. The mechanistic understanding of photoprotective processes in algae are mostly based on a limited number of model organisms, such as *Chlamydomonas reinhardtii* and *Phaeodactylum tricornutum*, as well as inference from observations in plants (e.g. Arabidopsis [*Arabidopsis thaliana*], *Nicotiana*, and *Triticum*). These species predominantly rely on nonphotochemical quenching (NPQ) to dissipate excess energy. This process becomes important for avoiding damage to the photosynthetic system when absorbed light energy cannot be fully utilized by the light-harvesting reactions. NPQ is triggered by a ΔpH gradient across the thylakoid membrane that leads to conformational changes in the light-harvesting antennae associated with PSII (Goral et al., 2012; Nicol et al., 2019).

Algae are a polyphyletic grouping of organisms and this is reflected in the varied light-harvesting antennae pigment–protein complexes utilized by algae, despite their similarities in the structure of PSII core proteins (Tokutsu and Minagawa, 2013; Pi et al., 2019). Additionally, different processes may fulfill the requirements for photoprotection in different taxa. For example, Streptophyte plants and the model Chlorophyte alga *C. reinhardtii* use the violaxanthin/antheraxanthin/zeaxanthin cycle to assist in the formation of NPQ. However, Stramenopile algae utilize a novel set of related carotenoids for the diadinoxanthin/diatoxanthin cycle for the same purpose (Demers et al., 1991). It is also possible that other photoprotective processes significantly contribute to photoprotection in algae such as alternative electron transport (AET; Houille-Vernes et al., 2011), PSII repair (Key et al., 2010), and photorespiration (Niyogi, 2000).

Desmodesmus armatus (strain SE 00107; previously referred to as *Scenedesmus armatus*) is an emerging alga of biotechnological interest. It has been demonstrated to detoxify wastewater and has resistance to high metal toxicity (Rugnini et al., 2017, 2018). *Desmodesmus* species have been shown to survive temperature fluctuations of 45°C for 24 h, with <13% heat-related mortality, and to flocculate readily inside ~2.5 h of settling (Pan et al., 2011; Chen et al., 2020). *D. armatus* naturally produces commercially valuable nutraceuticals such as lutein and lycopene and can accumulate lipids up to 50% of their dry-weight biomass (Pan et al., 2011).

[1]This work was supported by the U.S. Department of Energy (grant nos. DE–AC36–08GO28308 and DOE–DES0008595) and the National Institutes of Health (grant no. R25GM115300).

[2]Author for contact: graham.peers@colostate.edu.

[3]Senior author.

The author responsible for distribution of materials integral to the findings presented in this article in accordance with the policy described in the Instructions for Authors (www.plantphysiol.org) is: Graham Peers (graham.peers@colostate.edu).

M.A.W. and G.P. developed the project concept and experimental design; M.A.W. and D.H. carried out all physiology, biochemical, and biophysical experiments and analysis; M.C. developed the membrane inlet mass spectrometry setup and aided data collection and analysis; M.A.W. and G.P. wrote the article; all authors reviewed and contributed to the final version of the article.

[OPEN]Articles can be viewed without a subscription.

www.plantphysiol.org/cgi/doi/10.1104/pp.20.00373

All these factors contribute to its potential for deployment at a commercial scale.

Although *D. armatus* and other *Desmodesmus* species have been explored as a potential source for biomass, bioproducts, and biofuels (Sijil et al., 2019; Zhang et al., 2016), detailed photosynthetic characterization of this organism has not been performed. *D. armatus* possesses chlorophylls *a* and *b* (chl *a*/*b*) and the violaxanthin/antheraxanthin/zeaxanthin-cycle carotenoids (Tukaj et al., 2003). In the closely related species *Scenedesmus quadricauda*, NPQ is inhibited by the addition of dithiothreitol, suggesting this group likely utilizes a violaxanthin de-epoxidase–mediated NPQ (Masojídek et al., 1999).

There are other notable aspects of photophysiology that can minimize the overexcitation of PSII and maintain a maximum yield of PSII (ΦPSII) in excess light. Changes in the ratios of antennae proteins to reaction center core proteins, and thus pigment ratios, have been demonstrated in plants, *C. reinhardtii*, diatoms, and cyanobacteria in response to growth phase, culture/canopy densities, and light acclimation history (Schagerl and Müller, 2006; Murchie and Horton, 2008; Cantrell and Peers, 2017). Lower absorption cross sections simply capture less light per reaction center and reduce the probability of photodamage in excess light.

When algal blooms or mass cultures reach high cell densities, light limitation can occur. This leads to an increase in pigment per cell concentrations and in antennae proteins compared to core proteins (Neale and Melis, 1986). This ensures a higher probability of light capture. However, for productivity of mass culture, wasteful processes constitute huge losses to productivity (Melis, 2009; Andersson et al., 2019). Pigment reduction or truncated light-harvesting antennae proteins have been demonstrated to improve solar conversion efficiencies of mass cultures, while simultaneously reducing NPQ capacity and rates of photoinhibition in individual cells (Nakajima and Ueda, 1997; Melis, 2009). This was demonstrated in the truncated light-harvesting chlorophyll antenna size and in light-harvesting chlorophyll translator repressor *C. reinhardtii* mutants (Polle et al., 2003, Beckmann et al., 2009a).

AET is a collection of photoprotective mechanisms that are gaining greater prominence in algal photobiology research. AET is involved in light-independent and -dependent balancing of reductant. These processes utilize different forms of reductant (plastoquinol, NADPH) to reduce oxygen and produce water via the water–water cycle. The loss of AET proteins has been demonstrated to reduce photochemical quantum yields and growth rates in *C. reinhardtii* under intermittent-light conditions (Chaux et al., 2017; Nawrocki et al., 2019). Allahverdiyeva et al. (2013) as well as Andersson et al. (2019) have also shown AET to be an important photoprotective mechanism in cyanobacteria. Importantly, modifying the accumulation of AET-related proteins can improve photosynthetic efficiency and decrease photoinhibition in plants and cyanobacteria (Hasunuma et al., 2014; Yamamoto et al., 2016; Gómez et al., 2018). Together, this work suggests a prominent role for AET in photosynthesis and its application in bioengineering.

The efficient repair of excess-light–induced damages to the PSII reaction center (RCII) D1 protein is another mechanism to mitigate losses associated with photoinhibition (Key et al., 2010). PSII turnover occurs at all light intensities, and efficient repair rates are required to maintain a functional RCII when photosynthesis and photoprotective mechanisms are unable to utilize all energy absorbed by photosynthetic pigments (Tyystjärvi and Aro, 1996). Fast D1 protein repair rates can help maintain a high ΦPSII but cannot operate on the 10^{-15} s to 10^{-10} s timescales of photon capture and transfer that is required to minimize reactive oxygen species formation. There are also energetic costs required with the removal of damaged D1 protein and new protein synthesis (Theis and Schroda, 2016). Thus, PSII repair is not viewed as a classical photoprotective mechanism, but it is an essential process for maintaining maximum yields of photosynthesis and avoiding sustained photoinhibition.

Bioengineering of light harvesting and photoprotective mechanisms have been demonstrated to yield 15% increased biomass in plants (Kromdijk et al., 2016) and 28% in cyanobacteria (Peers, 2015). Engineering targets are, however, likely to be species- and cultivation-scenario–specific. The focus of this research is to better understand how *D. armatus* adapts to changing light. We sought to investigate how this organism balances light harvesting and energy dissipation between two major dissipative pathways (AET and NPQ), and what effect this has on ΦPSII and growth rates under light-limiting (LL), excess-light (HL), and simulated natural-light (SL) conditions. Here we show that *D. armatus* has a relatively small functional PSII antennae, high photoprotection capacities, and maintains high photochemical quantum yields throughout exponential growth phase. We elucidated the main photoprotective mechanism to be AET, despite the capacity to form limited NPQ. Furthermore, we reveal that *D. armatus* has a very efficient D1 repair rate that contributes to a high ΦPSII in HL conditions.

RESULTS

Growth in Square-Wave and SL Conditions

A preliminary group of experiments set out to characterize the growth stages of *D. armatus* (SE 00107) in several light conditions while growing in modified artificial saltwater media (MASM; see Supplemental Table S1 for composition). Cultures were grown under 12:12 h D:N HL (600 μmol photons m^{-2} s^{-1}), LL (60 μmol photons m^{-2} s^{-1}), and SL conditions (0–2,000 μmol photons m^{-2} s^{-1}; Supplemental Fig. S1). In all conditions, maximum growth rates were observed during the first 4 d, coinciding with the highest

maximum PSII photochemical yield (F_v/F_m) values and highest average chl a/b ratios (ranging from 6 to 7; Supplemental Table S2). This informed us that the exponential growth phase was within 1×10^5 to 1.5×10^6 cells mL^{-1}, and all subsequent experiments were performed during this time.

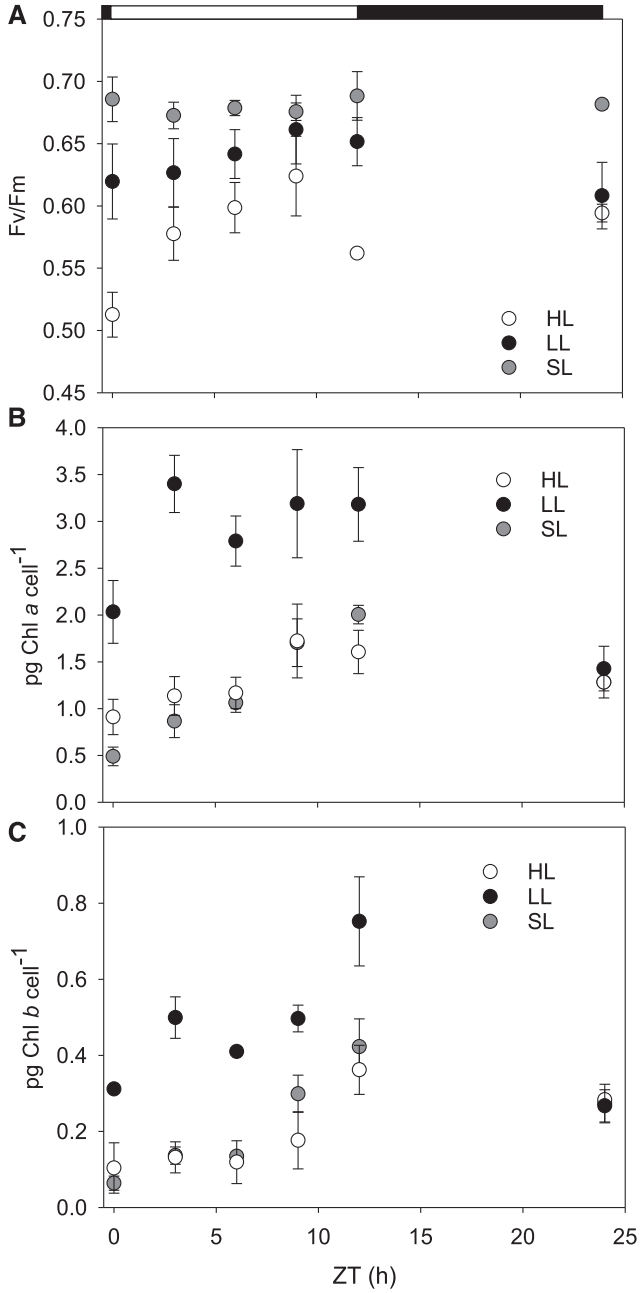

Figure 1. Estimations of F_v/F_m and chlorophyll pigment accumulation during a diurnal light cycle. Cultures were grown under HL, LL, or SL. A, In situ average F_v/F_m. B and C, Picograms of chl *a* (B) and chl *b* (C) per cell extracted in methanol and calculated spectrophotometrically. Error bars represent SD ($n = 3$). Open and filled horizontal bars indicate the light and dark phases of the diurnal light cycle.

F_v/F_m measurements show that LL-acclimated cultures maintain a high PSII quantum yield throughout the day without experiencing photoinhibition (Fig. 1). HL-acclimated cultures were photoinhibited during the first 30 min of illumination. This difference in maximum photochemical quantum yield was significantly lower than all other time points (Zeitgeber time [ZT]; repeated measures analysis of variance [RM-ANOVA], $P < 0.001$; Tukey's test, $P \leq 0.013$). The only other significant difference in F_v/F_m was at ZT 9 h to 3 and 12 h (Tukey's test, $P \leq 0.019$). F_v/F_m values of HL-adapted cultures were not otherwise significantly different between 3 and 24 ZT h.

SL-acclimated cultures had higher maximum photochemical quantum yields than HL-acclimated cultures at every time point during the day except ZT 9 h (Fig. 1; Tukey's test, $P \leq 0.014$). SL-conditioned cultures only had significantly higher maximum quantum yields than LL-acclimated cultures at ZT 0 and 24 h (Tukey's test, $P \leq 0.043$). All associated statistical test results are presented in Supplemental Table S3.

Pigment Content

The amount of chl *a* and *b* per cell increased between dawn and dusk in both diurnal square-wave light acclimation histories before declining during darkness (Fig. 1). LL-acclimated cells also had significantly higher chl *a* (RM-ANOVA, $P \leq 0.041$; Tukey's test $P \leq 0.08$) and chl *b* (RM-ANOVA, $P \leq 0.022$; Tukey's test, $P \leq 0.049$) quantities per cell at every time point during the photoperiod. Additionally, the chl *a/b* ratio was dynamic during the day in all conditions. Illustrating this, SL-acclimated cells had a chl a/b ratio of 7.92 ± 1.02 at solar noon before decreasing to 4.83 ± 0.74 (Supplemental Fig. S2, All associated statistical test results are presented in Supplemental Tables S4 and S5).

SL-adapted cells had a biphasic increase in chl *a* and *b* concentrations per cell throughout the daylight period (Fig. 1). Gradual increases in pigments were measured from ZT 0 h to ZT 6 h, with a large increase after solar noon. This strategy most closely mimicked HL-acclimated cells.

Estimations of PSII Supercomplex Functional Size in F_m' and F_m States

Measurements of functional antenna size in the dark-adapted state versus in the light-adapted state (in situ) suggested there was very little physiological adjustment of PSII size throughout the different growth conditions (Fig. 2). LL-acclimated cells had a slightly smaller average PSII functional absorption cross section (σPSII) than HL-acclimated cultures (Tukey's test, $P < 0.05$). We tested to see whether this was possibly due to a state-transition–like response whereby light-harvesting complexes migrate from one photosystem to the other. However, we were unable to observe state

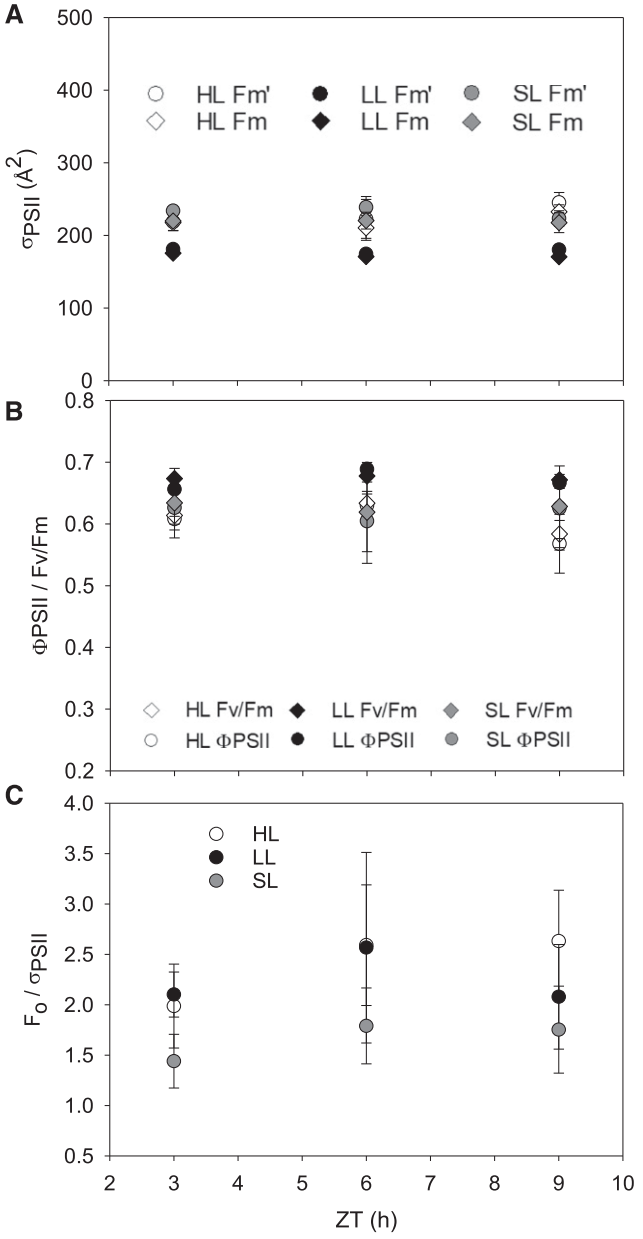

Figure 2. Estimations of σPSII), in situ PSII downregulation, and concentration of open RCIIs. Cultures were grown under HL, LL, or SL conditions. The in situ and dark adapted σPSII (A) was simultaneously measured with the in situ ΦPSII and dark-adapted F_v/F_m (B). Data denoted as F_m' correspond to ΦPSII, and F_m to F_v/F_m in A. C, Estimation F_o/σPSII in the F_m state. Error bars represent SD ($n = 3$).

transitions in the species (Supplemental Fig. S3). A slight peak at ~695 nm in the 77-K fluorescence emission spectra did suggest that there are some antennae proteins functionally uncoupled from PSII (Supplemental Fig. S3). Comparing in situ ΦPSII to dark-adapted F_v/F_m illustrated minimal downregulation of PSII efficiency due to photoinhibition or NPQ induction in both static light-acclimated conditions (Fig. 2). Despite little observed NPQ, the parameter F_o/σPSII shows no significant changes in the relative abundance of open RCII throughout the day (Fig. 2, RM-ANOVA $P > 0.1$). SL cultures did not display a notable deviation from these patterns. All associated statistical test results are presented in Supplemental Table S6.

Chlorophyll Fluorescence Dynamics

We tested if NPQ is present but not activated in situ, or if other photoprotective mechanisms are employed, by utilizing photosynthetic irradiance (P-I) protocols. These protocols allow us to simultaneously observe chlorophyll fluorescence kinetics along with photosynthetic gas exchange using membrane inlet mass spectrometry (MIMS). Chlorophyll fluorescence data showed that *D. armatus* does not exhibit a high NPQ capacity, no matter the acclimation history (Fig. 3). LL-acclimated cells did have the greatest NPQ capacity, with significantly higher NPQ than HL-acclimated cultures at 0 to 470 μmol photons m^{-2} s^{-1} (RM-ANOVA, $P \leq 0.019$; Tukey's test, $P \leq 0.022$, Supplemental Table S7)

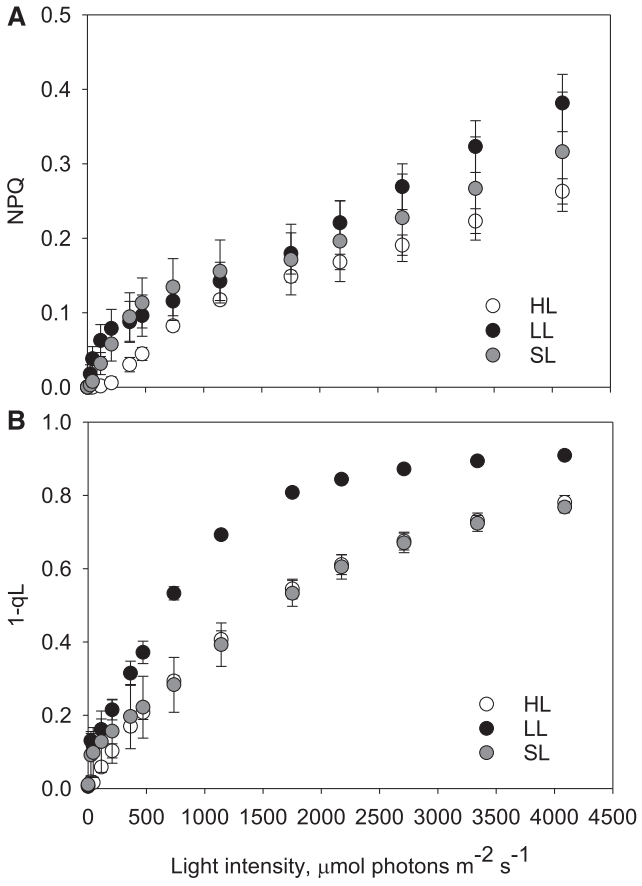

Figure 3. Redox state of the 1-qL and NPQ capacities of *D. armatus* cultures measured during an ex situ P-I curve. Cultures were grown under HL, LL, or SL conditions. NPQ (A) and 1-qL (B) were measured with a DUAL-PAM fluorometer. Two micrograms of chl *a* were loaded in a 1.4-mL total cuvette volume. Error bars represent SD ($n = 4$).

and at light fluxes >2,709 μmol photons m^{-2} s^{-1} (RM-ANOVA, $P \leq 0.038$ and Tukey's test, $P < 0.031$). Estimations of excitation pressure (1-qL) show that despite higher average total NPQ capacities, LL cells were not as effective at stopping the over-reduction of Q_A (Fig. 3). Indeed, differences in the 1-qL parameter show significant differences between LL- and HL-conditioned cells under all light intensities (RM-ANOVA, $P \leq 0.007$; Tukey's test, $P \leq 0.008$). At close to maximum incident sunlight intensities (~2,000 μmol photons m^{-2} s^{-1}), <60% of primary electron acceptors were in the reduced state in HL cultures (Fig. 3).

SL-acclimated cells had significantly lower NPQ capacity than LL-adapted cultures at 208 μmol photons m^{-2} s^{-1} (Fig. 3; Tukey's test, $P \leq 0.043$), and higher NPQ capacity than HL acclimated cells at 44 to 472 μmol photons m^{-2} s^{-1} (Fig. 3; Tukey's test, $P \leq 0.047$). Similarly to HL-grown cells, SL-grown cells required light intensities of >2,000 μmol photons m^{-2} s^{-1} to reduce most electron carriers (Fig. 3).

In a separate set of experiments, we also exposed cultures to conditions known to induce a large NPQ capacity in other green algae. SL-acclimated cells were grown into late stationary phase (chl *a*/*b* was <3.0). These were then assayed for NPQ capacity after 5 min of 750 μmol photons m^{-2} s^{-1} of actinic light (AL). These cells were then also treated with UV-B light as an additional method to induce NPQ capacity (Allorent et al., 2016; Supplemental Fig. S4). However, neither the stationary cultures nor stationary +UV-treated samples displayed significant NPQ ex situ, but UV treatment did cause a decline in F_v/F_m.

MIMS

We measured gas exchange using MIMS with exogenously added $^{18}O_2$, which allows for the observation of both oxygen evolution and consumption reactions in the light. Measurements of gross oxygen evolution show that the photosynthetic capacity of cells depended on acclimation history, with significant differences between conditions at every light intensity <208 μmol photons m^{-2} s^{-1} (Fig. 4, RM-ANOVA, $P \leq 0.027$, Supplemental Table S8). HL-acclimated cells had significantly higher gross oxygen evolution rates normalized to chl *a* than LL-acclimated cells (<208 μmol photons m^{-2} s^{-1}; Tukey's test, $P \leq 0.025$) or SL-acclimated cultures (<363 μmol photons m^{-2} s^{-1}; Tukey's test, $P \leq 0.045$). Oxygen consumption rates did not change significantly during the lowest light intervals (≤363 μmol photons m^{-2} s^{-1}), but once the light

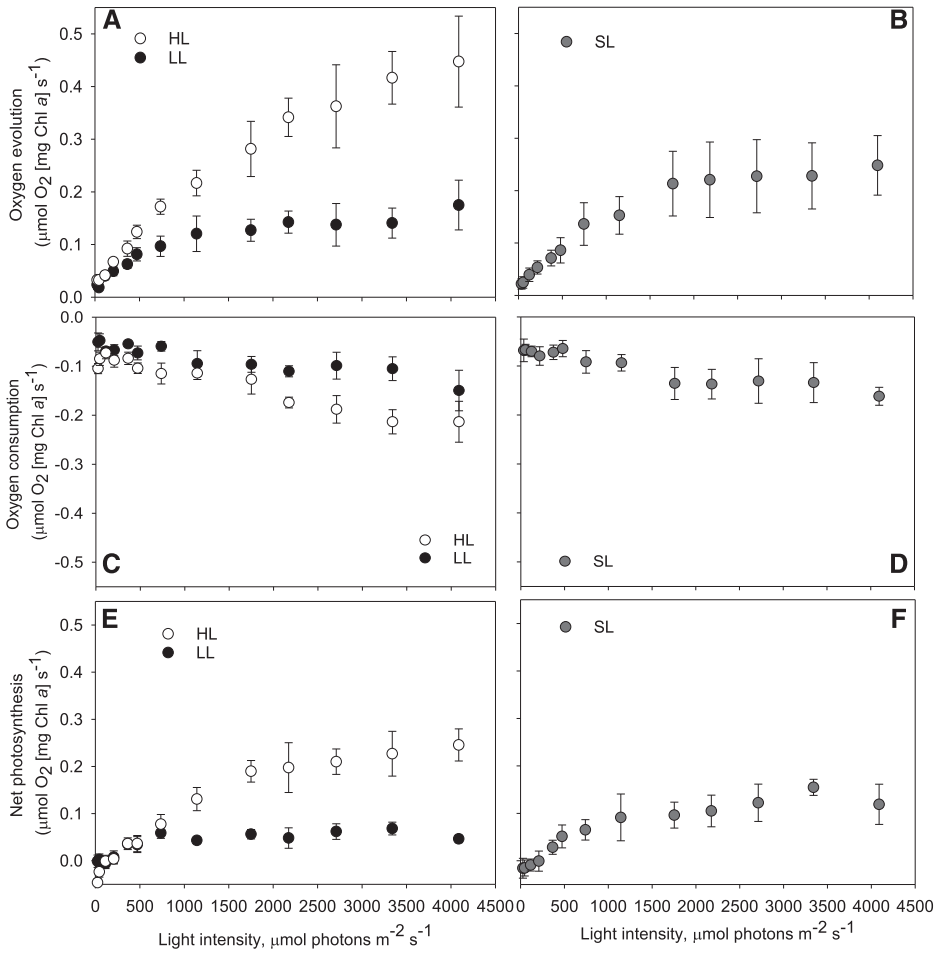

Figure 4. Ex situ estimations of oxygen evolution, consumption, and net photosynthesis capacity. Cultures were grown under HL, LL, or SL. Data were gathered simultaneously with that presented in Figure 3. A and B, Gross oxygen evolution. C and D, Gross oxygen consumption. E and F, Net photosynthesis. These were all measured using MIMS. Two micrograms of chl *a* were loaded in 1.4-mL total cuvette volume. Error bars represent SD ($n = 4$).

intensity reached ~470 μmol photons m^{-2} s^{-1}, there was an increase in average oxygen consumption at each AL interval (Fig. 4). HL-adapted cells have, on average, 3.4× higher net photosynthesis than LL cells, which illustrates the huge adaptation response in this organism. Significant differences between LL and HL cultures in the minimum saturating light intensity (P_{max}; Tukey's test, $P < 0.001$, Supplemental Table S9) and maximum rates of oxygen evolution (I_K; Tukey's test, $P < 0.001$) were also observed (Fig. 5).

Gross oxygen evolution rates were lower in SL-adapted cells than in HL-adapted cells at all light intensities. Oxygen consumption rates in SL cultures were similar to HL cultures, showing minimal changes between 0 and 470 μmol photons m^{-2} s^{-1}, but increasing at each AL interval after this. Net photosynthesis rates were not significantly different from LL-grown cultures throughout the P-I experiment.

Estimates of the maximal rate of photosynthesis suggests the pattern of HL < SL < LL (Fig. 5), but cells from all conditions were all able to harvest LL fluxes at equal efficiencies (alpha parameter; Tukey's test, $P \geq 0.052$; Fig. 5).

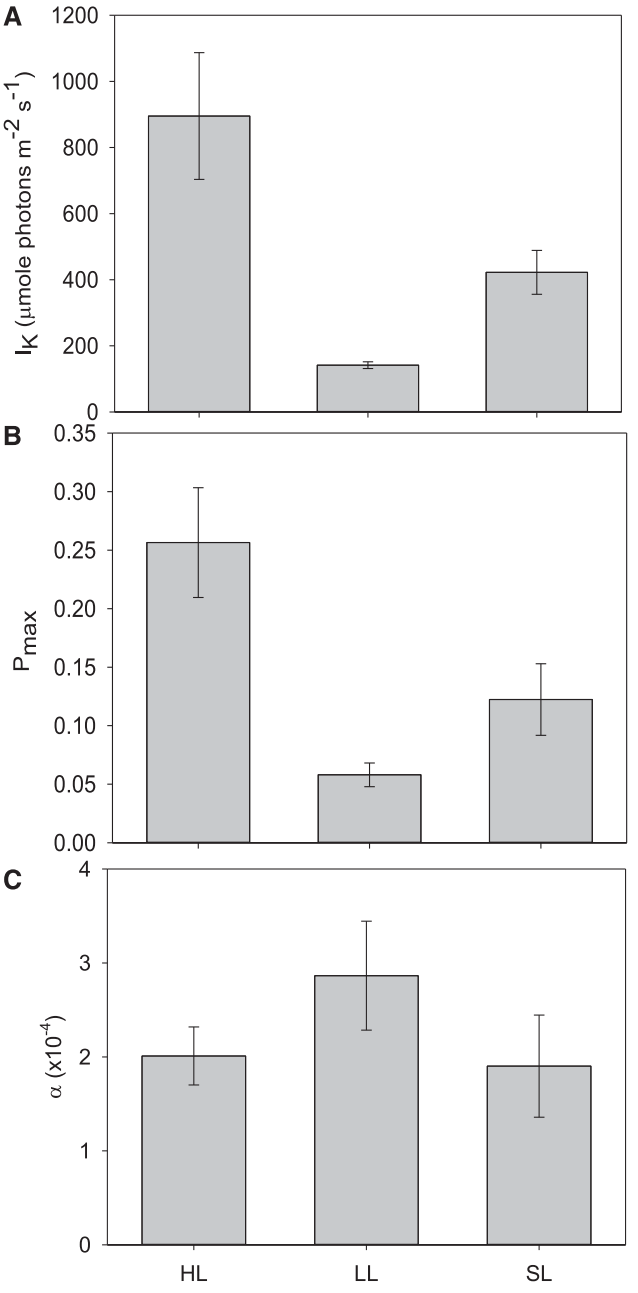

Figure 5. Estimations of photosynthetic performance characteristics (α, P_{max}, I_K) from net photosynthesis capacities calculated during an ex situ P-I curve. Cultures were grown under HL, LL, or SL. A, I_K represents the calculated minimum light intensity that causes saturation. B, P_{max} is the maximum predicted net photosynthesis capacity of each acclimated culture. C, α is indicative of the maximum photosynthetic efficiency as a function of oxygen evolution per photon. Error bars represent SD ($n = 4$).

Estimating In Situ Photosynthetic Capacities in Phenometrics Environmental Photobioreactors

We have previously modeled the light conditions experienced by individual cells in a phenometrics environmental photobioreactor (ePBR) system (see Andersson et al., 2019 for modeling details). We translated the output of this single-cell model at solar noon to a shortened script for employment on a DUAL-pulse–amplitude modulated (PAM) 100 fluorometer (Walz) coupled with MIMS (Supplemental Fig. S5). Estimations of PSII excitation pressure (1-qL) showed effective redox balancing of primary electron acceptors during rapid fluctuations in light (Fig. 6). The highest average 1-qL value observed during these fluctuations was 0.56, suggesting that 44% of acceptors are still in an oxidized state during rapid 0 to 2,000 μmol photons m^{-2} s^{-1} light transitions. Using a brief period of far-red light after illumination, the dark-measured qL (qL_d) average was 0.97, which infers that only 3% of RCII is permanently damaged and required a newly synthesized D1 protein. During these realistic solar-noon light fluctuations, NPQ was not significantly employed as a mode of excess energy dissipation, and the measured values only reached a maximum of ~0.2 (Fig. 6). MIMS-measured oxygen consumption rates showed that gross oxygen consumption was ~90% of gross oxygen production, greatly reducing net oxygen production (Fig. 6).

Dynamics of PSII D1 Protein Repair

Five-hundred micrograms per milliliter of the antibiotic lincomycin was applied to HL-acclimated cultures 20 min before dawn (ZT −0.33 h) to inhibit chloroplast-encoded D1 protein repair to distinguish synthesis rates from degradation rates (Key et al., 2010; Townsend et al., 2018). Figure 7 shows that D1 protein concentrations have visibly declined by ZT 30 min, with an absence of detectible protein by ZT 2 h. F_v/F_m is undermined in lincomycin-treated cultures 15 to 30 min

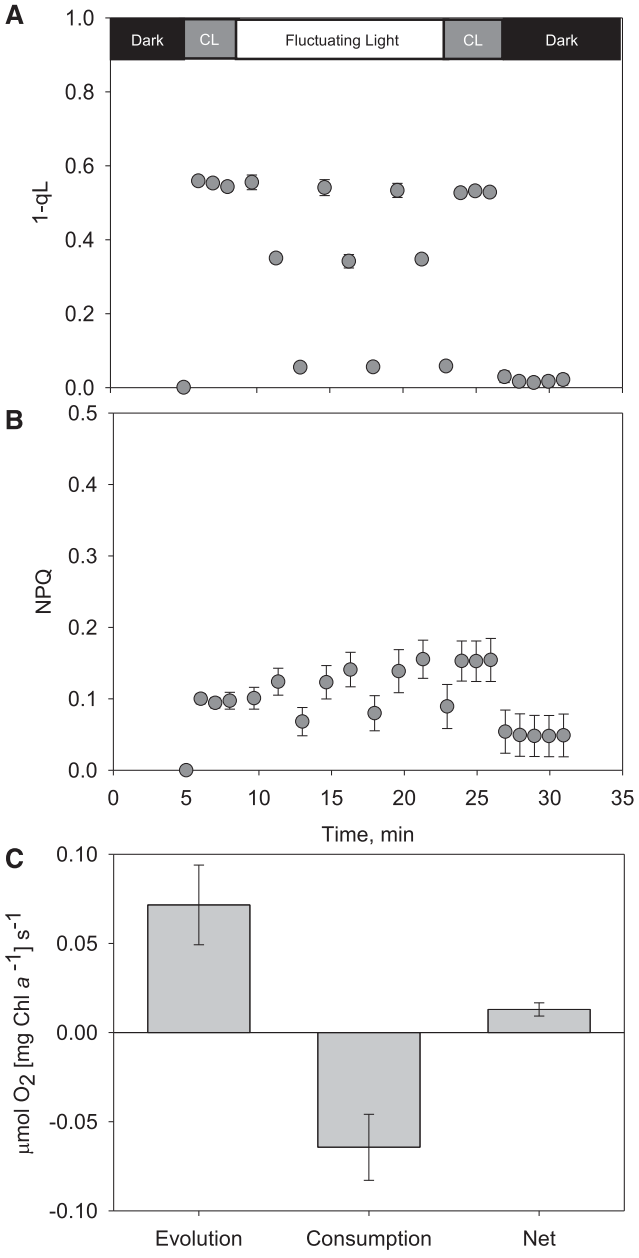

Figure 6. NPQ, 1-qL, and oxygen consumption, evolution, and net photosynthesis calculated during ex situ experiments replicating the in situ cell-specific light environment in a benchtop photobioreactor. A, Chl *a* fluorescence-based estimates of NPQ. B, One-qL parameters during an ex situ fluctuating-light experiment that models the cell-specific light environment of ePBR-grown cultures at solar noon (see Supplemental Fig. S5 for incident light data). C, Gross oxygen evolution, consumption, and net photosynthesis were measured simultaneously. Two micrograms of chl *a* were loaded in 1.4-mL total cuvette volume. Error bars represent SD ($n = 4$). CL, Constant light of 285 μmol of photons m^{-2} s^{-1}.

after dawn (Fig. 7) compared to untreated cultures. Analysis of the decline in F_v/F_m in lincomycin-treated cultures shows that by 42 and 210 min of 600 μmol photons m^{-2} s^{-1} light, 50% and >99% of PSII are damaged respectively (Fig. 7). Analysis of D1 protein western blots shows that intact D1 protein concentrations start decreasing at the same rates of F_v/F_m decline (Fig. 7).

DISCUSSION

D. armatus Dynamically Regulates Pigment Concentrations and Avoids Photoinhibition

To minimize the overexcitation of photosystems, algae can accumulate less pigment per cell, decrease their cell size, or change pigment ratios, which is indicative of a reduction in antenna size. Chlorophyte algae more commonly change ratios and employ state transitions, whereas diatoms reduce pigment concentrations and can functionally dissociate antennae proteins from core photosystem supercomplexes (Cantrell and Peers, 2017; Giovagnetti and Ruban, 2017). Here, *D. armatus* changed pigment per cell concentrations (Fig. 1) and chl *a*/*b* ratios (Supplemental Fig. S2) throughout a 24-h light period, like *C. reinhardtii*, but had significantly higher *a*/*b* ratios. Exponentially growing *D. armatus* had a very small antennae (chl *a*/*b* 6–10) until dusk (ZT 12 h), when chl *a*/*b* ratios declined to <5 (Supplemental Fig. S2). This happens regardless of light conditions. The decline in chl *a*/*b* ratio and decrease in pigment per cell during darkness occurs in conjunction with established diurnal circadian rhythms, including cellular divisions occurring at night in *D. armatus* (Supplemental Fig. S6; Matusiak-Mikulin et al., 2006). For comparison, *C. reinhardtii* grown under similar HL, LL, and SL conditions had chl *a*/*b* ratios of 2.76 to 3.49 (Cantrell and Peers, 2017), and engineered truncated light-harvesting antennae-protein mutants have chl *a*/*b* ratios of ~8.1 (Polle et al., 2003). It is worthwhile noting the unusual adaptation response in pigment ratio and quantity of *D. armatus* during its exponential growth phase. Chl *b* is almost exclusively located in the light-harvesting antennae, thus high chl *a*/*b* ratios indicate small antennae. This suggests that *D. armatus* produces significant amounts of RCII. This is a relatively costly investment, as RCII has more pigments and proteins than antennae complexes and requires continual replacement (discussed further below).

F_v/F_m showed little variation throughout the course of the day in SL- and LL-grown cultures. HL-acclimated cells were the only ones that exhibited photoinhibition at any time during the day, with a decline in PSII yields detected within the first 30 min of exposure to 600 μmol photons m^{-2} s^{-1}. This initial decline, however, was restored to maximum capacity by the next time point, indicating an efficient combination of photoprotection and D1 protein repair. We then proceeded to investigate the contribution of various potential mechanisms to maintaining a high ΦPSII in *D. armatus*.

Diurnal Changes in PSII Functional Antenna Size

Fluorescence induction and relaxation (FIRe) measurements offer a lot of photophysiological inferences

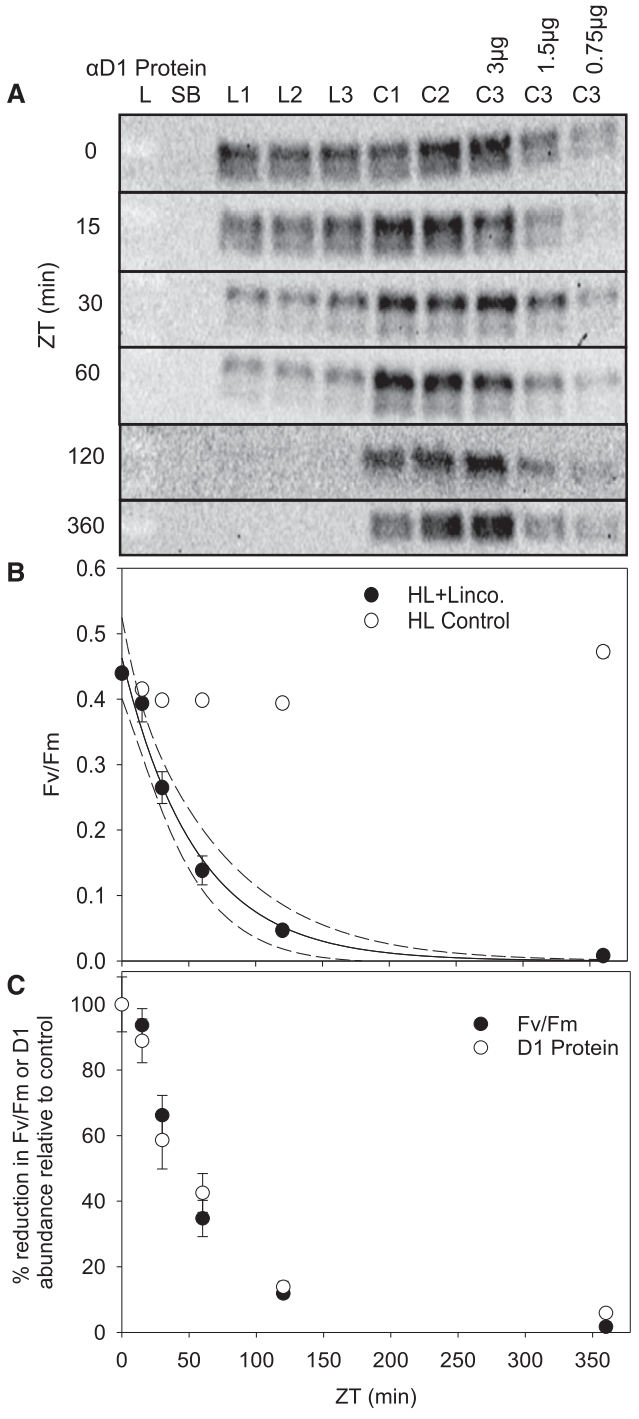

Figure 7. Estimation of D1 protein repair using lincomycin additions to HL-acclimated cultures at dawn. A, SDS-PAGE western-blot analysis of D1 protein using 3 μg of total protein and immunoblot detection of PsbA1 at various time-intervals post-dawn. L1 to L3 were treated as controls but with 500-μg mL^{-1} lincomycin added 15 min before dawn (ZT −15 min). C1 to C3 are independent cultures exposed to HL (600 μmol photons m^{-2} s^{-1}). Error bars represent SD (n = 3). L, Protein ladder; SB, sample buffer blank lane. B, F_v/F_m measured after 30-min dark adaptation. C, Relative decreases in the abundance of D1 protein abundance and F_v/F_m in lincomycin-treated cultures versus controls. Error bars represent SD (n = 3).

from PSII chl *a* fluorescence data that allow for estimations of PSII efficiency, size of PSII functional cross section, and F_m' quenching, and allow us to distinguish between the size and repair rates of PSII across different algal species (Key et al., 2010, Oxborough et al., 2012; Jallet et al., 2016a). We conducted measurements to coincide with solar noon (ZT 6 h) and to test whether midday suppression of PSII occurs, observed as lower F_v/F_m in diatoms, cyanobacteria, and vascular plants (Demmig-Adams et al., 1989; Jallet et al., 2016a; Andersson et al., 2019). Furthermore, we employed this tool to confirm the inference of a small antennae protein complex, based on the observed high chl *a*:*b* ratios (Fig. 1; Supplemental Fig. S2). These measurements showed that the functional cross section of *D. armatus* does not change drastically during the day and is much smaller (218–238 Å^2, Fig. 2) than *P. tricornutum*, which is ~400 Å^2 in SL conditions (Jallet et al., 2016a).

The induction of NPQ can dramatically increase or decrease the absorption cross section depending on the species (see Jallet et al., 2016a; Giovagnetti and Ruban, 2017 for examples). For instance, vascular plants increase the absorption cross section in the NPQ-state by 52% compared to the F_m state (Belgio et al., 2014). In contrast, *P. tricornutum* decreases absorption cross sections in the NPQ state by 48% to 57% from the F_m state (Giovagnetti and Ruban, 2017). The lack of an observable change in σPSII in the light- or dark-adapted states in this study suggested that NPQ is likely not induced in our culture conditions. Indeed, we did not observe in situ NPQ (Fig. 2). This agrees with the consensus that NPQ is predominantly located in the major antennae of chlorophytes and vascular plants (Goral et al., 2012; Nicol et al., 2019), and that *D. armatus* has a constitutively small antennae protein network.

These measurements suggest minimal in situ NPQ during the day, but they do not provide conclusive evidence for a lack of photoinhibition. Photochemical quantum yield measurements depend on F_o/F_o' and F_m/F_m'. NPQ affects both F_o' and F_m', and photoinhibition F_o' (Townsend et al., 2018). We utilized the F_o/σPSII parameter to estimate changes in active RCII. The ratio of F_o/σPSII has been used to infer the closure of reaction centers. Oxborough et al. (2012) demonstrated a linear positive correlation between F_o/σPSII and active RCII across chlorophytes and diatoms. Therefore, the lack of significant changes in F_o/σPSII from ZT 3 to ZT 9 suggests that the concentration of open reaction centers do not change (Fig. 2). In concert, chlorophyll fluorescence measurements suggest limited midday suppression of light harvesting and effective photoprotective processes in *D. armatus*.

Desmodesmus Does Not Have a Large Capacity for NPQ

NPQ is considered to be the major component of photoprotection in eukaryotic algae and plants. Many studies testing NPQ capacities utilize a LL to HL shift, or P-I measurements, which do not occur in mass culture conditions (Andersson et al., 2019). Jallet et al.

(2016a) illustrated that a high ex situ NPQ capacity does not mean a large in situ NPQ, even when grown under simulated natural-light regimes. We wanted to test whether in situ conditions here were also insufficient to activate NPQ, or whether NPQ is absent as a major photoprotective mechanism in this species. The P-I experiments illustrated that HL conditions were not enough to reduce all primary electron carriers in HL- and SL-acclimated cultures (measured as 1-qL, Fig. 3). This was correlated with a limited NPQ capacity of <0.4 (Fig. 3). For comparison, SL-grown *P. tricornutum* form the same amount of NPQ at 620 μmol photons m^{-2} s^{-1} as *D. armatus* cells do at 4,000 μmol photons m^{-2} s^{-1} (Jallet et al., 2016a). *C. reinhardtii* grown and assayed under similar LL, HL, and SL conditions have NPQ values of ~0.4, ~0.7, and ~1.0, respectively, at 1,850 μmol photons m^{-2} s^{-1} (Cantrell and Peers, 2017), whereas at 1,750 μmol photons m^{-2} s^{-1}, all conditions here yielded NPQ capacities of <0.2. These phenotypes are normally exhibited in mutants of other algal species that do not accumulate antennae proteins, and it agrees with NPQ capacities observed in closely related *Scenedesmus* species (Perales-Vela et al., 2007; Chalifour and Juneau, 2011; Ioannidis et al., 2011).

AET in *Desmodesmus*

Previous studies have found that AET can represent a large portion of total electron transport in a wide variety of algae and cyanobacteria (for examples, see Radmer and Kok, 1976). We estimated the capacity for AET by measuring light-dependent oxygen consumption of $^{18}O_2$ using MIMS. A large amount of light-dependent oxygen consumption significantly reduced the net oxygen production capacity of cells adapted to all light conditions (Fig. 4). Furthermore, as is common with photosynthetic organisms, parameters derived to measure photosynthetic efficiency and maximum productivity (Fig. 5) reflect acclimation history. The alpha parameter shows differences between all groups (RM-ANOVA, $P = 0.042$), but differences between HL- and LL-adapted cells were not significant (Tukey's test, $P = 0.084$) as in other organisms (Ware et al., 2015; Cantrell and Peers, 2017). Alpha is predominantly influenced by the functional antennae of supercomplexes, but LL conditions do not induce large antennae in *D. armatus* during the exponential growth phase. Despite the lack of significant acclimation-related changes in α, the P_{max} and I_K parameters change significantly (Fig. 5). Thus, this likely reflects differences in electron transport and carbon fixation processes that arise independently of antennae protein accumulation. Indeed, faster growth rates (Supplemental Table S1) and estimated electron transport rates (Supplemental Fig. S7) add support to these inferences from the P_{max} and I_K parameters.

AET Reduces Net Photosynthesis in Simulated Industrial-Light Conditions

Recent modeling of cell-specific light environments simulating industrially relevant SL conditions have demonstrated that light conditions in photobioreactors are highly dynamic and irregular. Andersson et al. (2019) illustrated that cells spend only ~25% of the day in the linear response range ($<P_{half\text{-}max}$), and the remainder in either LL or HL conditions, which significantly reduces photosynthetic efficiency compared to growth in the integrated average light intensity. Growth of photosynthetic algae in industrially relevant conditions has suggested that AET plays a more prominent role than NPQ in balancing the over-reduction of PSII (Jallet et al., 2016a; Andersson et al., 2019). Testing of NPQ capacity ex situ was required to rule it out as a major photoprotective process in this organism, but it might have suggested an exaggerated role for AET in situ. Thus, we utilized the light environment previously used by Andersson et al. (2019) to assay the utilization of AET versus NPQ in industrially relevant, in situ light conditions (ZT 6 h; Supplemental Fig. S5). These assays showed that HL fluctuations do not cause an over-reduction of Q_A and do not induce NPQ (Fig. 6). Instead, up to 90% of electrons generated by the splitting of water can be consumed by oxygen-consuming reactions downstream of PSII (Fig. 6), and they do not contribute to carbon fixation. Additionally, there is only minor photoinhibition in ~3% of RCII ($qL_d = 0.97$). This result suggests that AET engineering could improve photosynthetic efficiency at an industrial scale.

Several processes could contribute to the high rate of AET observed here. A recently published genome of *D. armatus* discovered the presence of genes that encode homologs of the terminal oxidases plastid terminal oxidase and Flavodiiron protein3 (Flv3; Knoshaug et al., 2020). FLVs has been shown to oxidize NADPH or NADH, reducing O_2 to water (Shimakawa et al., 2015). Additionally, expression of FLV proteins in tobacco (*Nicotiana tabacum*) and Arabidopsis, and over-expression of FLV proteins in *Synechocystis* sp. PCC6803, can increase carbon assimilation and improve photosynthetic efficiency, particularly in fluctuating-light conditions (Hasunuma et al., 2014; Yamamoto et al., 2016; Gómez et al., 2018). Plastid terminal oxidase proteins also contribute to chlororespiration and likely oxidize plastoquinol (Houille-Vernes et al., 2011; Krieger-Liszkay and Feilke, 2016). The biochemical modulation of these AET proteins is currently under debate. Additional proteins could also be involved in light-dependent AET, such as the following alternative oxidases: cytochrome *c* oxidase, quinol oxidase, and NADP-malate dehydrogenase (Scheibe, 2004; Jallet et al., 2016b).

Oxygen-consuming reactions could also include photorespiration. Plastidal glycolate glycerate translocator1-deficient mutant Arabidopsis accumulates $^{18}O_2$ in the chloroplasts that would otherwise be consumed producing 3-phosphoglycerate (Pick et al., 2013). South et al. (2019) suppressed PLGG1 and introduced more efficient glycolate metabolism to improve biomass in field tests by 20% compared to wild-type tobacco. Helman et al. (2005) attempted to parse light-dependent oxygen consumption and respiration. They estimated that respiration only

accounted for 6% of electron flow from PSII, and light-dependent oxygen consumed 40% of electron flow in cyanobacteria. *Phaeodactylum* spp. has also been estimated to consume up to 35% of oxygen generated at PSII in light-dependent AET reactions (Broddrick et al., 2019). Future research combining the use of inhibitors and reverse genetics will assist in teasing apart the exact nature of high AET in *Desmodesmus* spp.

D1 Protein Turnover Is Essential for Maintaining a High ΦPSII

HL-acclimated cells were chosen to investigate the dynamics of PSII repair, as previous measurements of F_v/F_m variance throughout the course of the day show that these conditions are enough to cause significant closure of PSII in the first hour after dawn (Fig. 1; ZT 0–1). Lincomycin infiltration is a useful tool, as it allows for the separation of photoprotective processes that function in maintaining a functional PSII from recovery processes that restore the damaged chloroplast-encoded D1 protein. We observed a decline in F_v/F_m and an ~90% reduction in D1 protein within 2 h of light exposure in lincomycin-treated cells (Fig. 7). We estimated that the half-life of the D1 protein in *D. armatus* is 42 min. This is significantly more rapid than has been observed for diatoms (Key et al., 2010). D1 protein turnover in spinach (*Spinacia oleracea*) illustrated a 30- to 120-min half-life and the rate was dependent on light acclimation history (Aro et al., 1993; Tyystjärvi et al., 1994). Because we observed nearly maximal F_v/F_m in HL and SL conditions, this suggests that *D. armatus* D1 protein capacity repair is fast and extremely efficient. It also suggests that the photoprotective processes described above are not completely adequate for preventing PSII from damage in HL conditions.

Although beyond the scope of this investigation, the rapid replacement of D1 proteins could be due to a combination of mechanisms. It has been suggested that certain algal species maintain a reserve of surplus PSII subunits to improve the efficiency of degradation and removal of damaged D1 proteins and reinsertion of functional polypeptides (Ni et al., 2017). It could also be due to an increase in transcriptional activity of the protease responsible for D1 protein degradation in HL, or an accumulation of FtsH proteases (Ni et al., 2017). An efficient D1 protein turnover, and thus restoration of ΦPSII, is a useful trait for biofuel platform species.

CONCLUSION

Vascular plants and many algae rely on NPQ to dissipate excess energy accumulated during HL or SL conditions. This work has established that *D. armatus* has three alternate but effective mechanisms to minimize the accumulation of damaged PSII: efficient D1 protein turnover, a constitutively small antenna, and AET. The first two characteristics are desirable for commercial production of algae, with reduction of antennae proteins reflecting a prominent target for bioengineering to increase photosynthetic efficiency (Polle et al., 2003; Melis, 2009). It was therefore encouraging to observe these properties in an organism already shown to have high productivities in mass culture. This work also adds support to our recent studies on *Synechocystis* sp. PCC 6803 (Andersson et al., 2019) and *P. tricornutum* (Jallet et al., 2016a), which suggest that NPQ is minimally employed by cells in light conditions that simulate mass culture, and that AET should be a focus of future algal bioengineering targets to increase photosynthetic productivity. Furthermore, SL-acclimated cultures had the highest maximum theoretical photochemical quantum yields, despite rapid changes in effective light intensities. Square-wave light regimes lead to PSII supercomplex arrangements that are not reflective of organisms in nature or growing in SL conditions (Ware et al., 2015), and this work bolsters the importance of studying photosynthetic organisms in simulated natural-light regimes.

MATERIALS AND METHODS

Growth Conditions and Treatments

Desmodesmus armatus (SE00107) was grown in MASM (at pH 8.0; for complete nutrient composition, see Supplemental Table S2). Constant light cultures were grown under 12-h day/night cycles with a custom-designed Dynamic Environmental Photosynthetic Imager white-LED light bank. HL corresponds to 600-μmol photons m^{-2} s^{-1} and LL to 60-μmol photons m^{-2} s^{-1} surface intensity measured with a light sensor (model no. ULM-500; Walz). Cultures were bubbled with atmospheric air (1 L air L^{-1} culture min^{-1}) and grown at 30°C. Samples were collected between ZT 5 h and ZT 7 h after dawn to simulate noon measurements, unless otherwise stated. For cultures grown under the SL regime in ePBRs, the LED lights were programmed to achieve a maximum 2,000-μmol photons m^{-2} s^{-1} surface light intensity at solar noon (see Supplemental Fig. S1) by the following equation:

$$\text{Incident Light Flux}(t) = A_{\max} * \sin(2 * \pi * f * t)$$

where t = s after dawn, $A_{\max}$ = 2,000 μmol photons m^{-2} s^{-1}, and $f = 1/(2 *$ Daylength[s]$) = 1.16 \times 10^{-5}$ s^{-1}.

SL-grown cultures were also bubbled with atmospheric air (1-L air L^{-1} culture min^{-1}) and grown at 30°C, with additional stirring (500 rpm). Samples were collected between ZT 5 h and ZT 7 h after dawn to simulate noon measurements, unless otherwise stated.

For lincomycin treatment, control and treated cultures were split in exponential phase. Three flasks were supplemented with 500 μg mL^{-1} of lincomycin 20 min before dawn, with three flasks were used for controls (Key et al., 2010). Biophysical measurements and western-blot analyses were performed on samples collected at 0, 15, 30, 60, 120, and 360 min after dawn (Key et al., 2010).

Cell Counts

Cell counts were performed on biological triplicates using a Micromaster microscope (Thermo Fisher Scientific) and an improved Bright-Line Neubauer hemocytometer (Sigma-Aldrich). For measurements performed during exponential growth phase, growth rates were calculated as $\ln[N_{t1}/N_{t0}] - [t_1 - t_0]$, where "ln" is the natural log of cell concentrations (N_t) and time (t), between sampling times 0 and 1.

Absorption Spectroscopy for Pigment Quantification

Ten milliliters of *D. armatus* cultures were harvested and centrifuged at 3,220*g* for 10 min. After discarding the supernatant, the pellet was frozen at −20°C

(Schumann et al., 2005 and references therein). Pellets were thawed and resuspended in aqueous 95% methanol, vortexed for 10 s, placed in a 72°C bead bath for 30 min being agitated every 10 min, placed in a fridge at 4°C for 15 min, and then centrifuged at 20,000*g* for 10 min (Sartory and Grobbelaar, 1984). Supernatants were transferred to 1.5-mL semimicro acrylic cuvettes with 1-cm path lengths. Absorption spectra were scanned from 300 to 800 nm, with 1-nm increments at a scan rate of 600 nm min^{-1} using a model no. 60 UV–Vis Agilent Spectrophotometer (Cary). Spectra were zeroed at 800 nm. Chlorophyll concentrations were calculated according to the extinction coefficients presented in Porra et al. (1989). Pigment extraction efficiency and comparative chl *b* degradation values were compared to methodologies outlined in Porra (1990, 2002; Supplemental Fig. S8).

Chlorophyll PAM Fluorescence and MIMS Analysis

A DUAL-PAM 100 Fluorometer (Walz), coupled with a quad mass spectrometer (model no. PTM28612 PrismaPlus QMS200; Pfeiffer), was employed for simultaneous chl *a* fluorescence and oxygen evolution and consumption measurements in a custom-made 2-mL glass cuvette with plastic stopper (see Andersson et al., 2019 for system details). Cells were harvested between ZT 5 h and ZT 7 h during the exponential growth phase, centrifuged (1,000*g*, 10 min), and then resuspended in fresh culture medium to reach a final chl *a* concentration of 1.4 μg chl *a* mL^{-1}. Samples were purged with N_2 until $^{16}O_2$ reached approximately half of atmospheric levels. Two milliliters of sample were then transferred to the cuvette and the stopper lowered to the sample meniscus. Here, $^{18}O_2$ (cat. no. 490474; Sigma-Aldrich) was then applied to the sample through the stopper. After ~5 min, once $^{18}O_2$ reaches a steady state that is greater than $^{16}O_2$, the stopper was lowered to purge any residual gas from the cuvette. Samples were maintained at 30°C during all steps using an Isotemp water bath (Thermo Fisher Scientific). Samples were illuminated with the measuring light (620 nm) for 30 s to allow for accurate determination of F_o. Saturating pulses of 635-nm light were applied at 10,000 μmol photons m^{-2} s^{-1} for 0.6 s. The rapid light curve function of the DUAL-PAM was used with 2 min of AL-intensity steps of 0, 24, 44, 113, 206, 363, 470, 736, 1,141, 1,751, 2,174, 2,709, 3,339, and 4,087 μmol photons m^{-2} s^{-1}. F_v/F_m, NPQ, 1-qL, and qL_d parameters were calculated as described in Kramer et al. (2004) and Ware et al. (2015). Rates of oxygen evolution and consumption were calculated with the following equations (Beckmann et al., 2009b):

$$\downarrow O_2 = \Delta^{18}O_2 \left(1 + \frac{[^{16}O_2]}{[^{18}O_2]}\right)$$

$$\uparrow O_2 = \Delta^{16}O_2 - \Delta^{16}O_2 \left(\frac{[^{16}O_2]}{[^{18}O_2]}\right)$$

where $[^{16}O_2]$ and $[^{18}O_2]$ reflect the ratios of $^{16}O_2$ and $^{18}O_2$ at the start of each 2-min AL illumination step. Oxygen concentrations were normalized to argon concentrations, chosen for similar solubility as O_2, to account for abiotic variance due to the MIMS gas consumption (Andersson et al., 2019). Ion current slopes were calibrated based on oxygen values for saturated and anoxic media values. Oxygen saturation was achieved by shaking 5 to 10 mL of media in a flask for 1 to 2 min. Anoxia was achieved by the addition of sodium dithionite to media. Values were normalized to chl *a* concentration. The minimum saturating light intensity (I_K), maximum photosynthetic rate (P_{max}), and the light limited slope (α) values were calculated by fitting net photosynthetic rates (μmol O_2 L^{-1} mg chl a^{-1} s^{-1}) versus irradiance (μmol photons m^{-2} s^{-1}) to the empirical functions of Platt et al. (1980) using the fitting analysis protocol of Ritchie (2008).

Estimations of NPQ and AET in Simulated Light Environments

We utilized the cell-specific light environment calculated for ePBRs as described by Andersson et al. (2019) to estimate what photoprotective processes are active in rapidly fluctuating light. Five min of darkness were used to measure respiration, before constant light of 285 μmol photons m^{-2} s^{-1}, which was the integrated photon flux intensity at solar noon. This was followed by three 5-min repeats of a rapidly fluctuating light script with saturating pulses applied every 100 s to measure F_o' and F_m' during the illumination procedure. Five min of constant light of 285 μmol of photons m^{-2} s^{-1} was applied after the dynamic AL illumination, before 5 min of darkness. See Andersson et al. (2019) for details associated with light quality and quantity. PAM fluorescence parameters and MIMS analysis were performed as described above.

Chlorophyll FIRe

Cells were collected at midmorning, noon, and midafternoon, corresponding to 3 to 3.5, 6 to 6.5, and 9 to 9.5 h after dawn (Jallet et al., 2016a). Two lots of a 200-μL sample were separately added to 1.8 mL of 30°C preheated MASM. One sample was immediately transferred to a sample cuvette for fluorescence analysis, whereas the other sample was dark-adapted for 15 min. A FIRe fluorometer (Satlantic) was used to measure ΦPSII or F_v/F_m (in light- and dark-adapted samples, respectively), with 450-nm excitation and 678-nm measured emission (Kolber et al., 1998; Jallet et al., 2016a). σPSII was calculated from raw fluorescence data using the program Fireworx (https://sourceforge.net/projects/fireworx/). The F_o/σ_{PSII} parameter was subsequently calculated according to Oxborough et al. (2012).

Protein Extraction, Quantification, and Visualization

Ten to 30 mL of culture were collected and centrifuged at 3,220*g* for 30 min at 4°C, with the resulting pellet resuspended in 1 mL of 18.2 MΩ water and frozen at −80°C until subsequent analysis was performed. One-hundred microliters of sample were added to 100 μL of denaturing sample buffer (final concentration: 125 mM of Tris HCl buffer at pH 6.8, 20% [v/v] glycerol, 4% [w/v] SDS, and 0.0025% [w/v] Bromophenol Blue). Homogenization was achieved by vortexing for 30 min with two stainless-steel beads. Samples were centrifuged at 20,000*g* for 10 min at 4°C. The supernatant was heat-treated for 5 min at 65°C (Jallet et al., 2016a) and then allowed to cool to room temperature. An aliquot was used for the quantification of extracted protein followed by using bovine serum standards and a BCA Protein Assay kit (Pierce), with the remainder being frozen at −80°C until further analysis.

SDS-Page Gel Electrophoresis and Immunoblotting

Once protein stock solutions reached room temperature, an aliquot was added to sample buffer to make 35 μL of 3 mg mL^{-1} of total protein. Twenty-five microliters were loaded into 10% to 20% Tris-Gly Gel (Novex). An XCell SureLock Mini-Cell System (Thermo Fisher Scientific) was used for gel electrophoresis according to the manufacturer's directions. Five microliters of protein ladder (catalog no. 26617; Thermo Fisher Scientific) were used for migration control, with 15 μL of sample buffer used as a control for antibody specificity. Migration was carried out in a Tris-Gly SDS Running buffer (25 mM of Tris base at pH 8.3, 192 mM of Gly, and 0.1% [w/v] SDS). Proteins were transferred to polyvinylidene difluoride membranes (Invitrolon) in a transfer buffer (12 mM of Tris at pH 8.3, 96 mM of Gly, and 20% [v/v] methanol) in an XCell II Blot Module (Thermo Fisher Scientific). Membranes were blocked overnight at 4°C in TBS (50 mM of Tris-Cl at pH 7.5 and 150 mM of NaCl) and 5% (w/v) skim milk. All the following steps were carried out at room temperature and under constant agitation: Membranes were challenged for 1 h with a PSII D1 protein antibody (catalog no. AS0584; Agrisera) diluted 1:10,000 in TBS with 0.5% (w/v) skim milk correspondingly. Three 5-min washes in TBS with 0.5% (w/v) skim milk followed. Here, 1:50,000 dilution of secondary antibody (horseradish-peroxidase–conjugated donkey anti-rabbit, catalog no. 31458; Pierce) in TBS with 0.5% (w/v) skim milk challenging was carried out for 1 h. Membranes were washed for four 5-min cycles in TBS with 0.5% (w/v) skim milk, and one 5-min wash in TBS, before application of SuperSignal West Femto Maximum Sensitivity Substrate (Thermo Fisher Scientific) for visualization (Jallet et al., 2016a). Total protein was visualized using SYPRO-Ruby according to the manufacturer's instructions (Thermo Fisher Scientific). Band densities were quantified using the software ImageJ, v. 1.48 (http://imageJ.nih.gov/ij/). Relative abundances were calculated by comparing band densities to the band detected at $ZT = 0$ h.

Low-Temperature Fluorescence Spectroscopy

HL-grown samples were induced into State II by incubating 10 mL of culture with 5 μM of carbonyl cyanide *p*-(trifluoromethoxy)phenylhydrazone in the dark for 25 min. State I was achieved by placing 10 mL of culture on a shaker in the presence of only far-red light for 1 h. Samples were collected, placed in a sample holder (catalog no. 5500031800; Horiba Jobin-Yvon), and immediately frozen in liquid nitrogen. Measurements were performed at 77 K using a

Fluorolog-3 spectrofluorometer (Horiba Jobin-Yvon) and Liquid Nitrogen Dewar (catalog no. FL-1013; Horiba Jobin-Yvon). Excitation was provided at 435 nm, with 1 nm of fluorescence spectral resolution with a spectral bandwidth of 5 nm. The baseline was subtracted at 750 nm and normalized to 682 nm.

Statistical Analysis

Statistical differences were tested by RM-ANOVA. Tukey's post hoc test was utilized to test differences between groups. A paired Student's *t* test was used to compare temporally separated measurements on the same samples in Figure 2. Statistical tests were all performed in the program SigmaPlot 13.0 (Systat Software). All values reported are means from three to six biological replicates ± SD.

Supplemental Data

The following supplemental materials are available.

Supplemental Figure S1. Surface light intensities of growth conditions examined.

Supplemental Figure S2. Chl *a*/*b* ratios of cultures based on pigment extractions performed in Figure 1, A and B.

Supplemental Figure S3. State-transition capacity of *D. armatus* using PAM fluorescence and 77K fluorescence spectroscopy.

Supplemental Figure S4. UV-B induced NPQ of sinusoidal light-acclimated cultures.

Supplemental Figure S5. Depiction of the fluctuating-light regime to estimate in situ NPQ and AET of sinusoidal light-acclimated cultures.

Supplemental Figure S6. Cell division synchronicity during a diurnal light cycle.

Supplemental Figure S7. Estimated electron transport rates from an ex situ P-I curve.

Supplemental Figure S8. Comparison of solvent extraction protocols in *D. armatus* and *C. reinhardtii*.

Supplemental Table S1. Nutrient composition of MASM.

Supplemental Table S2. Cell counts, F_v/F_m, and chl *a*/*b* ratios of HL-, LL-, and SL-acclimated cultures.

Supplemental Table S3. Maximum photochemical quantum yield (F_v/F_m) parameters for cultures with different acclimation histories and at different time points.

Supplemental Table S4. Chl *a* (picograms) per cell parameters extracted in aqueous methanol.

Supplemental Table S5. Chl *b* (picograms) per cell parameters extracted in aqueous methanol.

Supplemental Table S6. FIRe parameters calculated at ZT 3 h to ZT 9 h for cultures acclimated to different light conditions.

Supplemental Table S7. NPQ and 1-qL parameters calculated from ex situ P-I curves.

Supplemental Table S8. Oxygen evolution, consumption, and net photosynthesis parameters calculated from ex situ simultaneous MIMS and P-I curve induction experiments.

Supplemental Table S9. Alpha, P_{max}, and I_K parameters calculated from net photosynthesis capacities measured during ex situ simultaneous MIMS and P-I curve induction experiments.

Received March 26, 2020; accepted April 28, 2020; published May 26, 2020.

LITERATURE CITED

Allahverdiyeva Y, Mustila H, Ermakova M, Bersanini L, Richaud P, Ajlani G, Battchikova N, Cournac L, Aro E-M (2013) Flavodiiron proteins Flv1 and Flv3 enable cyanobacterial growth and photosynthesis under fluctuating light. Proc Nat Acad Sci USA **110:** 4111–4116

Allorent G, Lefebvre-Legendre L, Chappuis R, Kuntz M, Truong TB, Niyogi KK, Ulm R, Goldschmidt-Clermont M (2016) UV-B photoreceptor-mediated protection of the photosynthetic machinery in *Chlamydomonas reinhardtii*. Proc Natl Acad Sci USA **113:** 14864–14869

Andersson B, Shen C, Cantrell M, Dandy DS, Peers G (2019) The fluctuating cell-specific light environment and its effects on cyanobacterial physiology. Plant Physiol **181:** 547–564

Aro E-M, McCaffery S, Anderson JM (1993) Photoinhibition and D1 protein degradation in peas acclimated to different growth irradiances. Plant Physiol **103:** 835–843

Beckmann J, Lehr F, Finazzi G, Hankamer B, Posten C, Wobbe L, Kruse O (2009a) Improvement of light to biomass conversion by de-regulation of light-harvesting protein translation in *Chlamydomonas reinhardtii*. J Biotechnol **142:** 70–77

Beckmann K, Messinger J, Badger MR, Wydrzynski T, Hillier W (2009b) On-line mass spectrometry: Membrane inlet sampling. Photosynth Res **102:** 511–522

Belgio E, Kapitonova E, Chmeliov J, Duffy CDP, Ungerer P, Valkunas L, Ruban AV (2014) Economic photoprotection in photosystem II that retains a complete light-harvesting system with slow energy traps. Nat Commun **5:** 4433

Broddrick JT, Du N, Smith SR, Tsuji Y, Jallet D, Ware MA, Peers G, Matsuda Y, Dupont CL, Mitchell BG, et al (2019) Cross-compartment metabolic coupling enables flexible photoprotective mechanisms in the diatom *Phaeodactylum tricornutum*. New Phytol **222:** 1364–1379

Cantrell M, Peers G (2017) A mutant of *Chlamydomonas* without LHCSR maintains high rates of photosynthesis, but has reduced cell division rates in sinusoidal light conditions. PloS One **12:** e0179395

Chalifour A, Juneau P (2011) Temperature-dependent sensitivity of growth and photosynthesis of *Scenedesmus obliquus*, *Navicula pelliculosa* and two strains of *Microcystis aeruginosa* to the herbicide atrazine. Aquat Toxicol **103:** 9–17

Chaux F, Burlacot A, Mekhalfi M, Auroy P, Blangy S, Richaud P, Peltier G (2017) Flavodiiron proteins promote fast and transient O_2 photoreduction in Chlamydomonas. Plant Physiol **174:** 1825–1836

Chen Z, Shao S, He Y, Luo Q, Zheng M, Zheng M, Chen B, Wang M (2020) Nutrients removal from piggery wastewater coupled to lipid production by a newly isolated self-flocculating microalga *Desmodesmus* sp. PW1. Bioresour Technol **302:** 122806

Demers S, Roy S, Gagnon R, Viguanit C (1991) Rapid light induced changes in cell fluorescence and in xanthophyll-cycle pigments of *Alexandriura excavatum* (Dinophyceae) and *Thalassiosira pseudonana* (Bacillariophyceae): A photo-protection mechanism. Mar Ecol Prog Ser **76:** 185–193

Demmig-Adams B, Adams WW III, Winter K, Meyer A, Schreiber U, Pereira JS, Krüger A, Czygan FC, Lange OL (1989) Photochemical efficiency of photosystem II, photon yield of O_2 evolution, photosynthetic capacity, and carotenoid composition during the midday depression of net CO_2 uptake in *Arbutus unedo* growing in Portugal. Planta **177:** 377–387

Giovagnetti V, Ruban AV (2017) Detachment of the fucoxanthin chlorophyll *a*/*c* binding protein (FCP) antenna is not involved in the acclimative regulation of photoprotection in the pennate diatom *Phaeodactylum tricornutum*. Biochim Biophys Acta Bioenerg **1858:** 218–230

Gómez R, Carrillo N, Morelli MP, Tula S, Shahinnia F, Hajirezaei MR, Lodeyro AF (2018) Faster photosynthetic induction in tobacco by expressing cyanobacterial flavodiiron proteins in chloroplasts. Photosynth Res **136:** 129–138

Goral TK, Johnson MP, Duffy CDP, Brain APR, Ruban AV, Mullineaux CW (2012) Light-harvesting antenna composition controls the macrostructure and dynamics of thylakoid membranes in Arabidopsis. Plant J **69:** 289–301

Hasunuma T, Matsuda M, Senga Y, Aikawa S, Toyoshima M, Shimakawa G, Miyake C, Kondo A (2014) Overexpression of flv3 improves photosynthesis in the cyanobacterium *Synechocystis* sp. PCC6803 by enhancement of alternative electron flow. Biotechnol Biofuels **7:** 493

Helman Y, Barkan E, Eisenstadt D, Luz B, Kaplan A (2005) Fractionation of the three stable oxygen isotopes by oxygen-producing and oxygen-consuming reactions in photosynthetic organisms. Plant Physiol **138:** 2292–2298

Houille-Vernes L, Rappaport F, Wollman FA, Alric J, Johnson X (2011) Plastid terminal oxidase 2 (PTOX2) is the major oxidase involved in chlororespiration in *Chlamydomonas*. Proc Natl Acad Sci USA **108:** 20820–20825

Ioannidis NE, Sfichi-Duke L, Kotzabasis K (2011) Polyamines stimulate non-photochemical quenching of chlorophyll *a* fluorescence in *Scenedesmus obliquus*. Photosynth Res **107:** 169–175

Jallet D, Caballero MA, Gallina AA, Youngblood M, Peers G (2016a) Photosynthetic physiology and biomass partitioning in the model diatom *Phaeodactylum tricornutum* grown in a sinusoidal light regime. Algal Res **18:** 51–60

Jallet D, Cantrell M, Peers G (2016b) New players for photoprotection and light acclimation. In H. Kirchhoff, ed, Chloroplasts: Current Research and Future Trends. Caister Academic Press, Norfolk, UK

Key T, McCarthy A, Campbell DA, Six C, Roy S, Finkel ZV (2010) Cell size trade-offs govern light exploitation strategies in marine phytoplankton. Environ Microbiol **12:** 95–104

Knoshaug EP, Nag A, Astling DP, Douchi D, Laurens LML (2020) Draft genome sequence of the biofuel-relevant microalga *Desmodesmus armatus*. Microbiol Resour Announc **9:** e00896-e19

Kolber ZS, Prasil O, Falkowski PG (1998) Measurements of variable chlorophyll fluorescence using fast repetition rate techniques: Defining methodology and experimental protocols. Biochim Biophys Acta **1367:** 88–106

Kramer DM, Johnson G, Kiirats O, Edwards GE (2004) New fluorescence parameters for the determination of QA redox state and excitation energy fluxes. Photosynth Res **79:** 209–218

Krieger-Liszkay A, Feilke K (2016) The dual role of the plastid terminal oxidase PTOX: Between a protective and a pro-oxidant function. Front Plant Sci **6:** 1147

Kromdijk J, Głowacka K, Leonelli L, Gabilly ST, Iwai M, Niyogi KK, Long SP (2016) Improving photosynthesis and crop productivity by accelerating recovery from photoprotection. Science **354:** 857–861

Masojídek J, Torzillo G, Koblízek M, Kopecký J, Bernardini P, Sacchi A, Komenda J (1999) Photoadaptation of two members of the Chlorophyta (*Scenedesmus* and *Chlorella*) in laboratory and outdoor cultures: Changes in chlorophyll fluorescence quenching and the xanthophyll cycle. Planta **209:** 126–135

Matusiak-Mikulin K, Tukaj C, Tukaj Z (2006) Relationships between growth, development and photosynthetic activity during the cell cycle of *Desmodesmus armatus* (Chlorophyta) in synchronous cultures. Eur J Phycol **41:** 29–38

Melis A (2009) Solar energy conversion efficiencies in photosynthesis: Minimizing the chlorophyll antennae to maximize efficiency. Plant Sci **177:** 272–280

Murchie EH, Horton P (2008) Acclimation of photosynthesis to irradiance and spectral quality in British plant species: Chlorophyll content, photosynthetic capacity and habitat preference. Plant Cell Environ **20:** 438–448

Nakajima Y, Ueda R (1997) Improvement of photosynthesis in dense microalgal suspension by reduction of light harvesting pigments. J Appl Phycol **9:** 503–510

Nawrocki WJ, Buchert F, Joliot P, Rappaport F, Bailleul B, Wollman FA (2019) Chlororespiration controls growth under intermittent light. Plant Physiol **179:** 630–639

Neale PJ, Melis A (1986) Algal photosynthetic membrane complexes and the photosynthesis-irradiance curve: A comparison of light-adaptation responses in *Chlamydomonas reinhardtii* (Chlorophyta). J Phycol **22:** 531–538

Ni G, Zimbalatti G, Murphy CD, Barnett AB, Arsenault CM, Li G, Cockshutt AM, Campbell DA (2017) Arctic *Micromonas* uses protein pools and non-photochemical quenching to cope with temperature restrictions on photosystem II protein turnover. Photosynth Res **131:** 203–220

Nicol L, Nawrocki WJ, Croce R (2019) Disentangling the sites of non-photochemical quenching in vascular plants. Nat Plants **5:** 1177–1183

Niyogi KK (2000) Safety valves for photosynthesis. Curr Opin Plant Biol **3:** 455–460

Oxborough K, Moore CM, Suggett DJ, Lawson T, Chan HG, Geider RJ (2012) Direct estimation of functional PSII reaction center concentration and PSII electron flux on a volume basis: A new approach to the analysis of fast repetition rate fluorometry (FRRf) data. Limnol Oceanogr Methods **10:** 142–154

Peers G (2015) Enhancement of biomass production by disruption of light energy dissipation pathways. US Patent No. 8,940,508

Pan Y-Y, Wang S-T, Chuang L-T, Chang Y-W, Chen C-N (2011) Isolation of thermo-tolerant and high lipid content green microalgae: Oil accumulation is predominantly controlled by photosystem efficiency during stress treatments in Desmodesmus. Bioresour Technol **102:** 10510–10517

Perales-Vela HV, González-Moreno S, Montes-Horcasitas C, Cañizares-Villanueva RO (2007) Growth, photosynthetic and respiratory responses to sub-lethal copper concentrations in *Scenedesmus incrassatulus* (Chlorophyceae). Chemosphere **67:** 2274–2281

Pi X, Zhao S, Wang W, Liu D, Xu C, Han G, Kuang T, Sui S-F, Shen J-R (2019) The pigment-protein network of a diatom photosystem II-light-harvesting antenna supercomplex. Science **365:** 6452

Pick TR, Bräutigam A, Schulz MA, Obata T, Fernie AR, Weber AP (2013) PLGG1, a plastidic glycolate glycerate transporter, is required for photorespiration and defines a unique class of metabolite transporters. Proc Natl Acad Sci USA **110:** 3185–3190

Platt T, Gallegos CL, Harrison WG (1980) Photoinhibition of photosynthesis in natural assemblages of marine-phytoplankton. J Mar Res **38:** 687–701

Polle JEW, Kanakagiri S, Melis A (2003) *tla1*, a DNA insertional transformant of the green alga *Chlamydomonas reinhardtii* with a truncated light-harvesting chlorophyll antenna size. Planta **217:** 49–59

Porra RJ (1990) A simple method for extracting chlorophylls from the recalcitrant alga *Nannochloris atomus*, without formation of spectroscopically-different magnesium-rhodochlorin derivatives. Biochim Biophys Acta **1019:** 137–141

Porra RJ (2002) The chequered history of the development and use of simultaneous equations for the accurate determination of chlorophylls *a* and *b*. Photosynth Res **73:** 149–156

Porra RJ, Thompson WA, Kriedemann PE (1989) Determination of accurate extinction coefficients and simultaneous equations for assaying chlorophylls *a* and *b* extracted with four different solvents: Verification of the concentration of chlorophyll standards by atomic absorption spectroscopy. Biochim Biophys Acta **975:** 384–394

Radmer RJ, Kok B (1976) Photoreduction of O_2 primes and replaces CO_2 assimilation. Plant Physiol **58:** 336–340

Ritchie RJ (2008) Fitting light saturation curves measured using modulated fluorometry. Photosynth Res **96:** 201–215

Rugnini L, Costa G, Congestri R, Antonaroli S, Sanità di Toppi L, Bruno L (2018) Phosphorus and metal removal combined with lipid production by the green microalga *Desmodesmus* sp.: An integrated approach. Plant Physiol Biochem **125:** 45–51

Rugnini L, Costa G, Congestri R, Bruno L (2017) Testing of two different strains of green microalgae for Cu and Ni removal from aqueous media. Sci Total Environ **601–602:** 959–967

Sartory DP, Grobbelaar JU (1984) Extraction of chlorophyll *a* from freshwater phytoplankton for spectrophotometric analysis. Hydrobiologia **114:** 177–187

Schagerl M, Müller B (2006) Acclimation of chlorophyll *a* and carotenoid levels to different irradiances in four freshwater cyanobacteria. J Plant Physiol **163:** 709–716

Scheibe R (2004) Malate valves to balance cellular energy supply. Physiol Plant **120:** 21–26

Schumann R, Häubner N, Klausch S, Karsten U (2005) Chlorophyll extraction methods for the quantification of green microalgae colonizing building facades. Int Biodeterior Biodegradation **55:** 213–222

Shimakawa G, Shaku K, Nishi A, Hayashi R, Yamamoto H, Sakamoto K, Makino A, Miyake C (2015) FLAVODIIRON2 and FLAVODIIRON4 proteins mediate an oxygen-dependent alternative electron flow in *Synechocystis* sp. PCC 6803 under CO_2-limited conditions. Plant Physiol **167:** 472–480

Sijil PV, Sarada R, Chauhan VS (2019) Enhanced accumulation of alpha-linolenic acid rich lipids in indigenous freshwater microalga *Desmodesmus* sp.: The effect of low-temperature on nutrient replete, UV treated and nutrient stressed cultures. Bioresour Technol **273:** 404–415

South PF, Cavanagh AP, Liu HW, Ort DR (2019) Synthetic glycolate metabolism pathways stimulate crop growth and productivity in the field. Science **362:** eaat9077

Theis J, Schroda M (2016) Revisiting the photosystem II repair cycle. Plant Signal Behav **11:** e1218587

Tokutsu R, Minagawa J (2013) Energy-dissipative supercomplex of photosystem II associated with LHCSR3 in *Chlamydomonas reinhardtii*. Proc Natl Acad Sci USA **110:** 10016–10021

Townsend AJ, Ware MA, Ruban AV (2018) Dynamic interplay between photodamage and photoprotection in photosystem II. Plant Cell Environ **41:** 1098–1112

Tukaj Z, Matusiak-Mikulin K, Lewandowska J, Szurkowski J (2003) Changes in the pigment patterns and the photosynthetic activity during a light-induced cell cycle of the green alga *Scenedesmus armatus*. Plant Physiol Biochemi **41:** 337–344

Tyystjärvi E, Aro EM (1996) The rate constant of photoinhibition, measured in lincomycin-treated leaves, is directly proportional to light intensity. Proc Natl Acad Sci USA **93:** 2213–2218

Tyystjärvi E, Mäenpää P, Aro EM (1994) Mathematical modelling of photoinhibition and photosystem II repair cycle. I. Photoinhibition and D1 protein degradation in vitro and in the absence of chloroplast protein synthesis in vivo. Photosynth Res **41:** 439–449

Ware MA, Belgio E, Ruban AV (2015) Photoprotective capacity of non-photochemical quenching in plants acclimated to different light intensities. Photosynth Res **126:** 261–274

Yamamoto H, Takahashi S, Badger MR, Shikanai T (2016) Artificial remodelling of alternative electron flow by flavodiiron proteins in Arabidopsis. Nat Plants **2:** 16012

Zhang Y, He M, Zou S, Fei C, Yan Y, Zheng S, Rajper AA, Wang C (2016) Breeding of high biomass and lipid producing *Desmodesmus* sp. by ethylmethane sulfonate-induced mutation. Bioresour Technol **207:** 268–275